JOURNAL OF OPTOELECTRONICS AND ADVANCED MATERIALS, Vol. 10, No. 9, September 2008, p. 2213 - 2222

Semiconductor photoelectrodes for solar of splitting water

E. INDREA*, S. DREVE, D. T. SILIPAS, G. MIHAILESCU, L. OLENIC, A. PETRU, V. DANCIU[a], V. COSOVEANU[a], A. NICOARA[a], L. E. MURESAN[b] , E. J. POPOVICI[b], V. POPESCU[C] , N. HOREA-IUSTIN[c], V. R. TETEAN[d], G. L. BAIA[d], T. NYARI[e]

National Institute for Research and Development of Isotopic and Molecular Technologies, Donath 71 – 103, 400293 Cluj-Napoca, Romania
[a]Babes-Bolyai University, Faculty of Chemistry and Chemical Engineering, 1 M. Kogalniceanu, 400028 Cluj-Napoca, Romania
[b]Raluca Ripan Institute for Research in Chemistry , 30 Fantanele, 400294 Cluj-Napoca, Romania
[c]Technical University of Cluj-Napoca, 15 C. Daicoviciu, 400020 Cluj-Napoca, Romania
[d]Babes-Bolyai University, Physics Faculty, 1 M. Kogalniceanu, 400028 Cluj-Napoca, Romania
[e]National Institute for Research and Development in Electrochemistry and Condensed Matter, 144 A.Podeanu, 300860 Timisoara, Romania

The production of hydrogen from water using solar light is very promising for generation of an ecologically pure energy carrier. Different types of TiO_2 aerogels have been successfully synthesized and the sample with the highest BET surface area was morphologically characterized with the help of SEM measurements. A series of ZnO / TiO_2 aerogels were prepared by the sol-gel method followed by supercritical drying. By varying the ZnO quantity (1-10 %) and the nature of Zn precursors - zinc (II) nitrate hexahydrate and zinc (II) acetylacetonate, an extensive study has been performed. We try to extend the photoresponse by introducing defects into the TiO_2 lattice by doping with transition metal ions Fe and Ni. Noble metals, in particular silver, has been used to increases the photocatalytic capacity of titania.

(Received February 25, 2008; accepted August 14, 2008)

Keywords: Electrode materials, Chemical synthesis, Microstructure, X-ray diffraction

1. Introduction

In its simplest form, a photoelectrochemical (PEC) hydrogen production cell consists of a semiconductor electrode and a metal counter electrode immersed in an aqueous electrolyte. When light is incident on the semiconductor electrode, it absorbs part of the light and generated electricity. This electricity is then used for the electrolysis of water.

Fujishima and Honda first demonstrated the lyses of water using solar energy in a PEC cell about 30 years ago [1]. The PEC cell consists of a semiconductor photo anode which is irradiated with the electromagnetic radiation. The counter electrode is a metal. Following processes take place in the cell when light is incident on the semiconductor electrode:

1. Photo generation of charge carriers (electron and hole pairs);

2. Charge separation and migration of the holes to the interface between the semiconductor and the electrolyte and of electrons to the counter electrode through the external circuit. Now, holes are simply vacancies created in the valence band due to promotion of electrons from the valence band to the conduction band;

3. Electrode processes: oxidation of water to H^+ and H_2O by the holes at the photo anode and reduction of H^+ ions to H_2 by electrons at the cathode.

The energy of 1.23 eV per electron transferred corresponds to a wavelength of λ=1008 nm.

However water does only absorb solar radiation in the infrared where photon energies are too low to drive the photochemical splitting of water. Thus any photochemical process to drive this reaction must involve a sensitizer, that is a molecule or semiconductor that can absorb sunlight and which ultimately leads to the generation of hydrogen.

Semiconductor systems differ from photochemical systems in the sense that sunlight is absorbed by a semiconductor material, and creates excess electrons in the conduction band and excess holes in the valence band. If this semiconductor contains a junction (e.g. a p-n) junction the chemical potential of the excess carriers can be converted into electricity, as is done in photovoltaic cells. Alternatively the excess electrons and/or holes can undergo chemical reactions at the surface of the

semiconductor to produce chemicals that can store the photon energy, like hydrogen gas produced from water.

There is a growing awareness that titania (TiO_2) and TiO_2-based oxide systems are the most promising candidates for the development of photoelectrodes for photoelectrochemical cell (PEC) for solar-hydrogen production [2].

Because of their ultra low density and high surface area, TiO_2 aerogels are attractive for their applications in solar energy conversion [3].

The effective band gap of a TiO_2 semiconductor can be reduced by adsorption of a dye on the surface of the semiconductor, which is capable of adsorption in the visible region of the solar spectrum.

Porphyrin dyes are very effective in capture of solar visible radiation. In the literature are described also the properties of some ruthenium-pyridyl compounds, as very effective dyes used in photoelectrochemical processes [4]. At present light-induced processes in covalently-linked multicomponent systems containing porphyrin are of great interest [5].

A major drawback of TiO_2 is the large bandgap of 3.2 eV, so wavelengths below 400 nm are necessary for excitation, which limits the photosensivity to the UV part of the solar spectrum. In order to improve the quantum yield and the spectra sensitivities of TiO_2-based photocatalysis, the $e^- - h^+$ recombination as to be reduced and the band gap as to be decreased. Many efforts have been made in these directions. In general, there are three ways to achieve the separation of e^- and h^+ and to extend the photoresponse : (a) by modifying TiO_2 by surface deposition of noble metal clusters [6-8]; (b) by coupling TiO_2 with other semiconductors possessing favorable band gaps and potentials like TiO_2–SnO_2 [9,10]; (c) by introducing defects into the TiO_2 lattice by doping with transition metal ions, e.g. Cu, Co, Fe, Cr, Ni, Pd, Pt, Eu [11-15].

2. Experimental details

2.1. Preparation of nanostructured TiO_2 aerogels

Aerogels are nanostructurated materials, unique by their properties, having complex microstructure characterized by very low densities, high surface area and porosity. TiO_2 aerogels combine the aerogel properties with the photocatalytical property of the titania that explains the researchers' interest for their potential applications such as photocatalysts with high efficiency in chemical synthesis and environmental depollution.

TiO_2 gels were prepared with the acid (HNO_3)-catalyzed sol-gel method by using titanium isopropoxide (TIP), HNO_3, EtOH and H_2O with different molar ratios as presented in Table 1.

Table 1. The BET surface area and total pores volume for different TiO_2 aerogel types obtained from various molar ratios of the used precursors.

TiO_2 aerogel type	Molar Ratio TIP / H_2O / EtOH / HNO_3	BET Surface Area	Total Pore Volum
		m^2/g	cm^3/g
I	1 / 3.675 / 21 / 0.08	593	1.97
II	1 / 3.50 / 23.33 / 0.08	466	1.1
III	1 / 3.50 / 18.66 / 0.08	383	1.24

The gels were allowed to age in the mother liquor for at least 40 days. Before drying, the gels were successively washed with excess of fresh alcohol, at least four times and were kept in alcohol from a week to several months. TiO2 aerogels were obtained by supercritical evacuation of solvent from gels prepared by acid-catalyzed sol-gel method [16]. The as prepared TiO_2 aerogels were subjected to a heat treatment at 300, 350, 450, 475, 500, 550 and 600 ^oC.

2.2. Synthesis and purification of porphyrin-bipyridyl supramolecular assembly

In order to extend the band of absorption in the visible domain of the TiO2-based oxide systems the coupling of tetra-pyridil-porphyne (TPyP) with tris-(2, 2'-bipyridyl)ruthenium(II)chloride ($Ru(bpy)_3Cl_2$) in a supramolecular assembly was performed. The classical synthesis strategy of the supramolecular assembly was adopted following the indications found in the literature [17,18]. The procedure consist in refluxing for 3h a hydro-alcoholic ($EtOH/H_2O$ 9:1 v:v) solution of bi-pyridine-phosphonate with of tris-(2, 2'-bipyridyl)ruthenium(II)chloride (cis-$[Ru(bpy)_3 Cl]_2$ x $2H_2O$). The solvents were removed in rotary evaporator and the residue was dissolved in a minimum volume of water/acetone (9:1 v:v), and it was poured in a silicagel column. In order to remove the unreacted $Ru(bpy)_3Cl_2$ the column was washed with a acetone/water (8:2 v:v) eluent. The pure fractions of supramolecular complex was collected with acetone, and the final solution was dried in normal conditions. The solid fraction of supramolecular assembly was redissolved in a hydro-alcoholic ($EtOH/H_2O$ 9:1 v:v) solution. All the reagents were Sigma Aldrich pure grade.

2.3. ZnO-TiO_2 aerogels synthesis

ZnO-TiO_2 aerogels were obtained by sol-gel method followed by supercritical drying. The acid catalyzed sol-gel process was carried out under normal conditions. Two different solutions were prepared. A first solution contained tetra-iso-propyl ortotitanate - TIP (Merck;

>98%), in ½ ethanol volume and a second one Zn $(NO_3)_2$ $6H_2O$ (Merck) or zinc acetylacetonate (Zn $(AcAc)_2$ Merck) dissolved in ethanol, doubly distilled water, nitric acid (Merck) and ½ ethanol volume. After homogenizing, the first solution was slowly added to the second under vigorous stirring. The corresponding molar ratios are presented in Table 2.

The resulted gels were covered and allowed to age for several months at room temperature. After three times washing with ethanol, the gels were dried by low-temperature supercritical drying with liquid CO_2 using a SAMDRI - PVT -3D dryer (Tousimis Res.Corp.USA). The as obtained aerogels were calcined at 773 K for 2h in the air, using a CARBOLITE furnace, and characterized.

Table 2. Reactant molar ratios used to ZnO-TiO_2 aerogel synthesis.

No.	Sample TiO_2-ZnO_2	Molar ratios						Gelation time	Gel aspect
		TIP	EtOH	H_2O	HNO_3	$Zn(NO_3)_2$	$Zn(AcAc)_2$		
1	ZnN1	1	20,39	3.698	0.079	0.100	-	5-7 min	semiopaque
2	ZnN025	1	19.14	3.549	0.079	0.025	-	5-7 min	translucid
3	ZnN01	1	20,64	3.694	0.079	0.010	-	3-5min	translucid
4	ZnA1	1	20,04	3.694	0.079	-	0.100	10 days	pale yellow translucid
5	ZnA05	1	20,35	3.694	0.079	-	0.050	50 min	pale yellow translucid
6	ZnA01	1	20,61	3.694	0.079	-	0.010	5-7 min	pale yellow translucid

2.4. Sol-gel preparation of the metal (Fe, Ni, Ag) doped TiO2-aerogels

The acid catalyzed sol-gel process was carried out under normal conditions. Two different solutions were prepared. A first solution contained tetra-iso-propyl ortotitanate - TIP (Merck; >98%) in ½ ethanol and a second one metal salt dissolved in ethanol, doubly distilled water, nitric acid and 1/2 ethanol. After homogenizing, the first solution was quickly added to the second one under vigorous stirring. The corresponding molar ratios are presented in Table 3. The resulted gels were covered and allowed to age for several months at room temperature. The alcohol was then removed by low-temperature supercritical drying with liquid CO_2 using a SAMDRI - PVT -3D dryer (Tousimis Res.Corp.USA). The as obtained aerogels were calcined at 773 K for 2h in the air, using a CARBOLITE furnace, and characterized.

Table 3. Experimental conditions of the metal doped TiO_2 aerogels synthesis.

Me- TiO_2	Molar ratio				Gelation time [min]
	$[Me(NO_3)_x]$ / $[Ti(OC_3H_7)_4]$	$[C_2H_5OH]$ / $[Ti(OC_3H_7)_4]$	$[H_2O]$ / $[Ti(OC_3H_7)_4]$	$[HNO_3]$ / $[Ti(OC_3H_7)_4]$	
Ag-TiO_2	0.04468	21	3.675	0.08	10
Ni-TiO_2	0.01459				10
Fe-TiO_2	0.01459				15

We study the influence of the gelification time, the nature and the concentration of the doping metal ion and the UV-irradiation time on the photocatalytic efficiency of transparent mesoporous metal doped titania thin films, made by a sol-gel method involving reverse micellar templates [19].

2.5. Experimental techniques

The TEM images were collected with a JEOL 200CX electronic microscope with a field emission tip that operated at 10 kV. A drop of the TiO_2 nanometric powder alcoholic suspensions was deposited on carbon –coated TEM grid and allowed to dry before investigation.

The surface area of the as prepared samples was determined by the BET method, in a partial pressure range of $0.05 < P/P_0 < 0.3$. The nitrogen adsorption was carried out at 77 K. Before each measurement the samples were heat-cleaned at 333 K for 2h. The total pore volume (V_{TP}) was obtained from the N_2 adsorption isotherm at a partial pressure of 0.98.

The hidroalcoholic 10^{-5} M solutions of TPyP, $Ru(bpy)_3Cl_2$ and $Ru(bpy)_3Cl_2$ + TPyP assembly were prepared by dissolving Sigma Aldrich pure grade chemicals in EtOH/H_2O 1:1 v:v solution. The solutions were freshly prepared and kept in the dark before measurements. Ultraviolet and visible absorption spectra were taken with a ABL&JASCO V500 spectrophotometer

using a 1.0 cm quartz cuvette versus a blank hidroalcoholic reference. Spectra were registered digitally under the control of the program Spectra Analysis associated to the equipment, running on PC. The absorption spectra for the TiO_2 photoanode surface immersed in 10^{-5} M solution of supramolecular assembly $Ru(bpy)_3Cl_2$ + TPyP and dried was recorded versus a dye-free TiO_2 photoanode surface. In both cases the photoanode TiO_2 layers were supported on a 2.5 x 2.5 cm ITO glass plate (UQG Optics Ltd. U. K.).

Small Angle X-ray Scattering (SAXS) is a very useful tool to investigate the changes in morphology of aerogels on preparation parameters [20]. The (SAXS) intensities were obtained by using homemade vacuum-sealed small-angle goniometer mounted on a standard DRON-3M diffractometer, working at 45 kV and 30 mA, and equipped with scintillation counter with single channel pulse height discriminator counting circuitry. The X-ray source (Cu K_α , λCuK_α = 1.54178 Å, Ni filtered), equipped with a bent graphite monochromator yields a monochromatic, collimated and focused beam. The data of the SAXS scattering intensities were collected in a step-scanning mode with $\Delta 2\theta = 0.01^0$ steps and then transferred to a PC for processing. Accumulation times were 100s/step and the measurements were performed at room temperature. The aerogels were placed as a 20μm thick layer in a vacuum-thight stainless steel sample holder closed by two mica windows of thickness 10μm.

SAXS intensities I(s) were recorded as function of the modulus of scattering vector $s=4\pi\sin\theta/\lambda$, 2θ being the scattering angle, in the s range from s_0 = 0.19 to s_m= 4.4 nm^{-1}. The data were corrected by the parasitic scattering and sample attenuation and normalized by the beam intensity and the sample thickness. Scattering data were corrected for background, slit smearing [21], and sample thickness.

The X-ray diffraction patterns were obtained by using a standard DRON-3M powder diffractometer, working at 45 kV and 30 mA, and equipped with scintillation counter with single channel pulse height discriminator counting circuitry. The Cu K_α (λCuK_α = 1.54178 Å) radiation, Ni filtered, was collimated with Soller slits. The data of the X-ray diffraction patterns were collected in a step-scanning mode with $\Delta 2\theta = 0.025^0$ steps and then transferred to a PC for processing.

3. Results and discussion

3.1. TiO_2 aerogels

Because of their ultra low density and high surface area, TiO_2 aerogels are attractive for their applications in solar energy conversion. Nanocrystalline semiconductor films are constituted by a network of mesoscopic TiO_2 particles witch are interconnected to allow for electronic conduction to take place. The nanoporous TiO_2 layer has a high specific surface area; this increases the contact of the photoelectrode surface with light and therefore amplifies the light harvesting efficiency of the cell. The band gap of the TiO_2 is approximately 3.2 eV. There are three main crystalline phases of TiO_2: anatase, rutile and brookite. Rutile is the easiest to produce because it is thermodynamically most stable. TiO_2 aerogels were obtained by supercritical evacuation of solvent from gels prepared by acid-catalyzed sol-gel method [22].

According to characteristics, and porosity of the nanostructured titanium dioxide specific applications were developed [23]. We investigated the morphology of TiO_2 aerogels using SAXS combined with wide-angle X-ray diffraction (WAXD). The main reason for our choice is that the distribution of scattered intensity over a small and wide-angle range allows us to estimate two relevant morphological parameters: information about the relative internal surface of grains and pores and estimation of crystallite size, respectively.

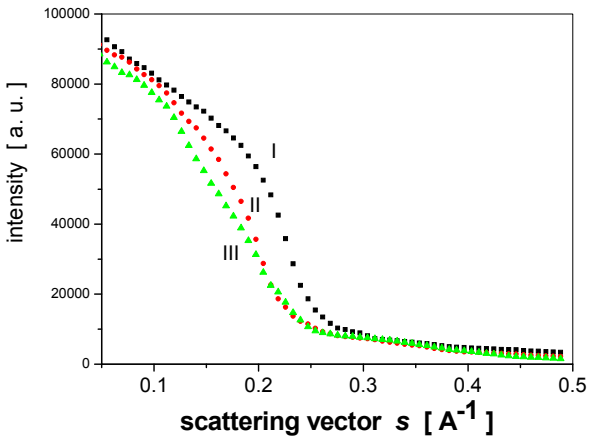

Fig.1. The curves of the SAXS intensity, I(s), as a function of the scattering vector s for the scattering from I, II and II aerogel samples, after supercritical drying.

Scattering data were corrected for background, slit smearing [24], and sample thickness.

For nonfractal aerogels exhibiting a Porod law, information about specific surface area has been obtained by describing the aerogels as a two phase medium [25].

The SAXS intensity within the low-q range produced by an isotropic set of uncorrelated particles dispersed in a homogenous matrix can be described by Guinier law and gives the characteristic radius of gyration R_g parameter [25]. Oscillations in the Porod law domain have been analyzed by plotting $I(q)\cdot q^4$ vs. q and the specific surface area was calculated using the skeletal density value.

A computer program package named PRIMUS (Windows PC-based system for small-angle scattering data analysis) [26], directly applied to the scattering curves,

yields the Guinier radius of gyration, the specific surface area and the distribution function of the spheres.

The radius of gyration Rg and forward scattering I(0) are computed using the Guinier approximation and the Porod invariant Q and Porod volume V of the particle are evaluated using the Porod approximation [26]. The angular range for computation can be adjusted interactively for the Guinier plot (Fig.2.a) , whereby the Porod constant K is automatically calculated from the Porod asymptote [I(s)s4 versus s4] at higher angles (Fig.2.b) [26]. The specific surface area per unit volume of sample was determinated from the Porod invariant and was found in good agreement with BET surface area, determined by gas adsorption (Table 4).

Table 4. The BET surface area and total pores volume for different TiO_2 aerogel types obtained from various molar ratios of the used precursors.

Aerogel samples	Thermic teatment	Guinier radius of gyration R_g R_g [nm]	Porod radius of gyration R_p [nm]	Specific SAXS surface area per unit volume of sample [m^2 / g]	Specific BET surface area per unit volume of sample BET [m^2 / g]
I	as obtined	9.3	9.6	562	593
II	as obtined	14.8	15.1	402	466
III	as obtined	19.2	19.6	312	383

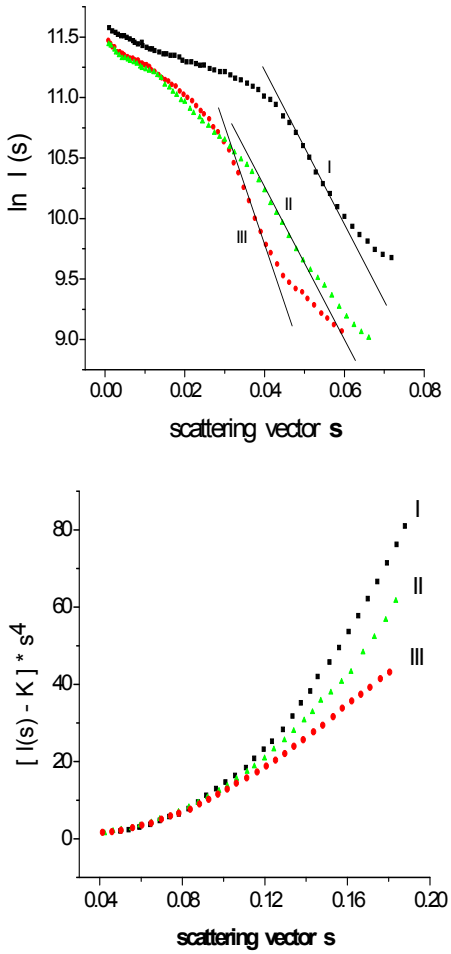

Fig.2. The SAXS angular range for computation for aerogel samples I, II and III adjusted interactively for the Guinier plot (a) ; the Porod constant K is automatically calculated from the Porod asymptote [I(s)s4 versus s4] at higher angles (b).

3.2. The structure of porphyrin and bipyridyl compounds

The structure of porphyrin and bipyridyl compounds [27, 28] allow the absorption of visible solar radiation, as is revealed by the UV-VIS spectra of TPyP and [Ru(bpy)$_3$ Cl]$_2$, presented in Fig.3.a and Fig.3.b.

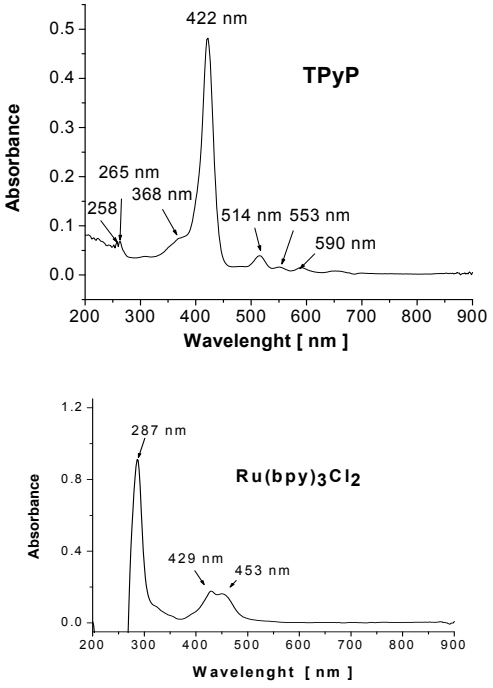

Fig. 3. UV-VIS spectra of a) tetra-pyridil-porphyne (TPyP) and b) tris-(2,2'-bipyridy l)rutenium(II)chloride (cis-[Ru(bpy)$_3$ Cl]$_2$ x 2H_2O).

The UV-VIS spectra of TPyP in ethanol solution is mainly determined by transitions within the π system of the tetrapyrolic macrocycle, characteristic to the

aromaticity of all porphyrins, having a Soret band at 422 nm, and three Q bands at 514, 553 and 590 nm. The presence of two bands at 258 and 265 nm and of the shoulder of 368 nm are attributed to the electronic interactions between the pyridyl groups and the porphyrin main skeleton [28].

The UV – VIS spectra of cis-$[Ru(bpy)_3\ Cl]_2$ x $2H_2O$ presents a band at 287 nm, attributed to the electronic effects due to the pyridyl groups, and two bands at 429 nm and 423 nm due to the π-π^* intramolecular transitions of the bipyridyl groups.

The control of the complex formation and the determination of their stoichiometry were carried out according to Job's method [28]. The most probable structure of the ($Ru(bpy)_3Cl_2$ + TPyP) assembly is reproduced in Fig.4.

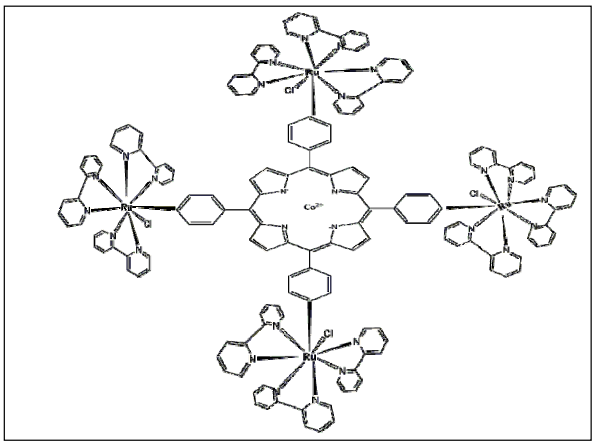

Fig. 4. Most probable molecular structure of the supramolecular porphyrin-bipyridyl-rutenium ($Ru(bpy)_3Cl_2$ + TPyP) assembly.

The purpose of extending the absorption band of visible light, in order to assure a larger domain for the water-splitting process, was realized by immersing TiO_2 photoanode in solutions of a supramolecular assembly tris-(2, 2'-bipyridyl)ruthenium(II)chloride ($Ru(bpy)_3Cl_2$) with tetra-pyridil-porphyne (TPyP), two important dyes of the chemistry of photoelectrochemical process involved in solar water-splitting. The results are in good agreement with the literature data [29].

After the separation and the purification of the supramolecular assembly $Ru(bpy)_3Cl_2$ + TPyP the UV-VIS spectra of the solution was recorded, as is presented in Fig. 5a.

The TiO_2 photoanode surface was immersed in 10^{-5} M solution of supramolecular assembly, it was dried in normal conditions, and the UV-VIS absorption bands were determined, as is reproduced in Fig.5b.

The UV – VIS spectra of the supramolecular species in hidroalcoholic solution were similar to the sum of the ruthenium complex and corresponding porphyrin spectra, as shown in Fig. 5. The $Ru(bpy)_3Cl_2$ + TPyP spectrum has a Soret band at 427 nm, a Q band at 521 nm, and the three bands at 240, 289 and 358 nm, corresponding to pyridyl global interactions with the system. The absorption of supramolecular assembly $Ru(bpy)_3Cl_2$+TPyP onto nanocrystalline TiO_2 leads to active red-brown films with an continuous extended band in the visible region between 340-450 nm.

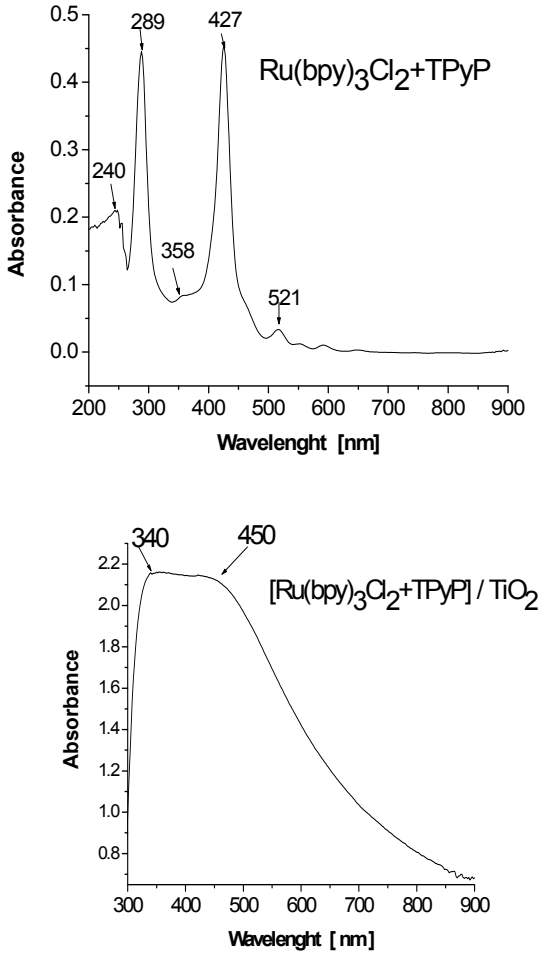

Fig. 5. Absorption bands in UV-VIS range for a) 10^{-5} M hidroalcoholic solutions of $Ru(bpy)_3Cl_2$ + TPyP and b) TiO_2 photoanode surface immersed in 10^{-5} M solution of supramolecular assembly $Ru(bpy)_3Cl_2$ + TPyP and dried.

3.3. The structure of the ZnO-TiO_2 aerogels

A serie of ZnO-TiO_2 aerogels were prepared by the sol-gel method followed by supercritical drying. By varying the ZnO quantity (1-10 %) and the nature of Zn precursors - zinc (II) nitrate hexahydrate and zinc (II) acetylacetonate see Table 2), an extensive study has been performed.

The X-ray powder diffraction technique was used for structural characterization of the ZnO-TiO_2 aerogels.

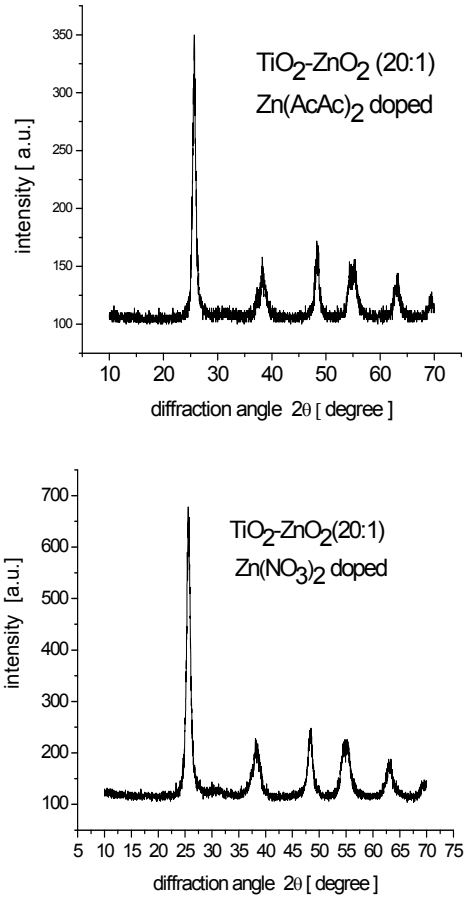

Fig. 6. X-ray diffraction patterns for the nanostructured ZnO-TiO_2 aerogels – ZnN01 (a) and ZnA01 (b) samples.

Fig. 6 shows the X-ray diffraction patterns resulting by the analysis of the heat-treated ZnO-TiO_2 aerogels and suggests the formation of a anatase-like crystalline network structure with a = b = 0.37(8) nm and c = 0.95(7) nm lattice parameters, quite close to the ASTM reported values. Unit cell parameters were calculated through Rietveld refinement using the PowderCell software [30].

The microstructural information obtained by the single X-ray profile Fourier analysis of the ZnO-TiO_2 aerogels were: the D_{eff}(nm) effective crystallite mean size, the $<\varepsilon^2>^{1/2}_{hkl}$ root mean square (rms) of the microstrains averaged along [hkl] direction and the dislocation density ρ [31,32].

The Warren-Averbach X-ray profile Fourier analysis of the (400) and the (440) TiO_2 anatase peak profiles were processed by a XRLINE [32] computer program.

Table 5 summarizes the microstructural parameters of the ZnN1, ZnN025, ZnN01, ZnA1, ZnA05 and ZnA01 aerogel samples .

The microstructural parameters of the nanocrystalline ZnO-TiO_2 aerogels showed a average size of the TiO_2 anatase of 8 nm to 10 nm when they were prepared by the sol-gel method with zinc (II) nitrate hexahydrate precursors and of 10 nm to 18 nm when they were prepared with zinc (II) acetylacetonate precursors and was found in good agreement with BET surface area, determined by gas adsorption (see Table 5).

Table 5. Lattice parameters a=b, c and the microstructural parameters, the D_{eff}(nm) effective crystallite mean size, the $<\varepsilon^2>^{1/2}_{hkl}$ root mean square (rms) of the microstrains , the dislocation density ρ and BET surface area of the ZnN1, ZnN025, ZnN01, ZnA1, ZnA05 and ZnA01 aerogel samples .

No.	Sample TiO_2-ZnO_2	a [Å]	c [Å]	D [nm]	$<\varepsilon^2>^{1/2} \times 10^{-2}$	$\rho \times 10^{14}$ (lines m^{-2})	Particle/air interface surface area BET [m^2 / g]
1	ZnN1	3.810(9)	9.597(9)	8.2	0.451	1.070	134
2	ZnN025	3.805(3)	9. 590(7)	8.7	0.358	0.800	121
3	ZnN01	3.794(6)	9.581(5)	10.0	0.330	0.642	112
4	ZnA1	3.818(8)	9.644(4)	10.2	0.413	0.788	117
5	ZnA05	3.804(6)	9.574(3)	14.5	0.367	0.492	77
6	ZnA01	3.787(9)	9.517(5)	18.1	0.308	0.331	9.1
	Anatase	3.784	9.514				

Fig.7 shows the effective crystallite size distribution D_{eff} (L) and root mean square (rms) of the lattice microstrain $<\varepsilon^2>^{1/2}$ (L) distribution in the real anatase crystallites space for nanocrystalline ZnO-TiO_2 aerogels, ZnA1, ZnA05 and ZnA01 aerogel samples.

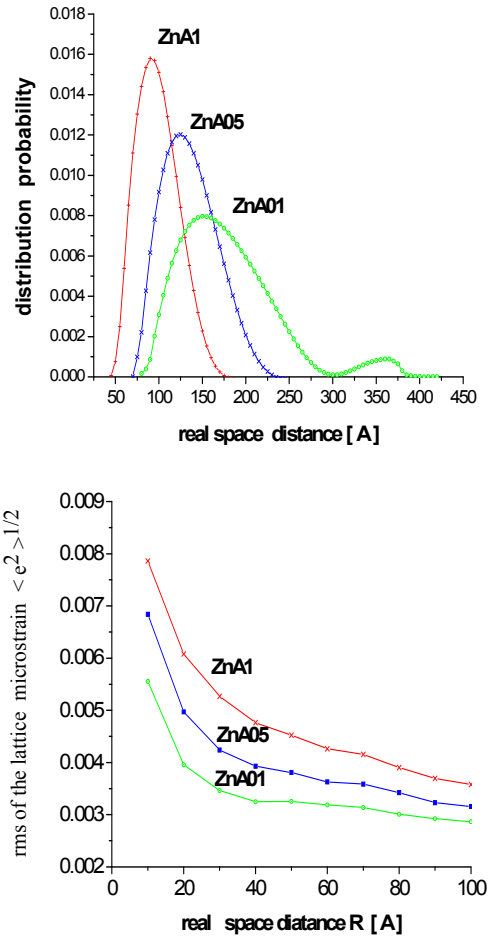

Fig.7. The effective crystallite size D_{eff} (L) distribution (a) and root mean square (rms) of the lattice microstrain $< \varepsilon^2 >^{1/2}$ (L) distribution (b) in the real anatase crystallites space for nanocrystalline ZnO-TiO_2 aerogels , ZnA1, ZnA05 and ZnA01 aerogel samples samples.

3.4. Metal doped (Fe, Ni, Ag) titania thin films

In order to improve the quantum yield and the spectra sensitivities of TiO_2-based photocatalysis, e.g. the $e^- - h^+$ recombination has to be reduced and the band gap has to be decreased, we try to extend the photoresponse by introducing defects into the TiO_2 lattice by doping with transition metal ions Fe and Ni. Noble metals, in particular silver, has been used to increases the photocatalytic capacity of titania by some different physical mechanisms that may act separately or simultaneously, e.g. reduced silver particles of colloidal dimension (metallic silver) are considered to be electron scavengers.

Mesoporous metal doped titania thin films, made by a sol-gel method are structured in nanoparticles of controlled and uniform size, both in pure form or doped with silver, nickel and iron. The metal ions were introduced in the films by initial solubilization in the reverse micellar solution.

The microstructure of the samples investigated by TEM (Fig. 8-10) shows a relatively compact microstructure with small micropores (individual and non-communicating) but without macropores. The microporosity varies as a function of the metal ions content and the increasing doping leads to an important decrease of pore size and interconnectivity. XRD patterns revealed a major anatase phase mixed with a brookite fraction. XRD measurements show that the lattice parameter c of anatase phase decreases with dopant addition, while the value of a remains essentially unchanged.

In the TiO_2:Fe doped films (Fig. 8) it can be presumed that Fe^{3+} substitutes Ti^{4+} preferentially on the body centered and face centered lattice sites in the anatase structure, since only the axial parameter c changes, while a remains the same. This result is very important for photocatalytic activity since only substitutional dopants can act directly as trapping sites to enhance the carrier lifetime.

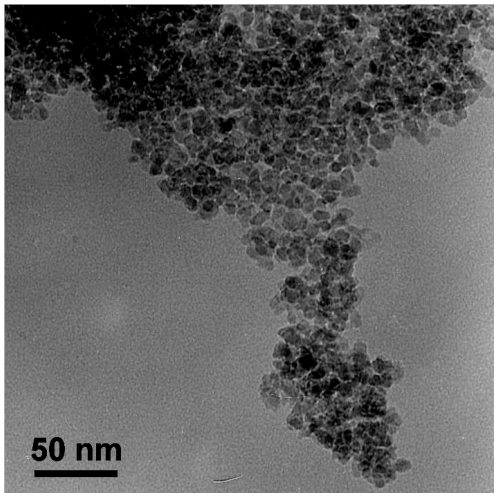

Fig. 8. TEM image of the doped TiO_2:Fe aerogel . The mesospheres dimension is of about 11 nm.

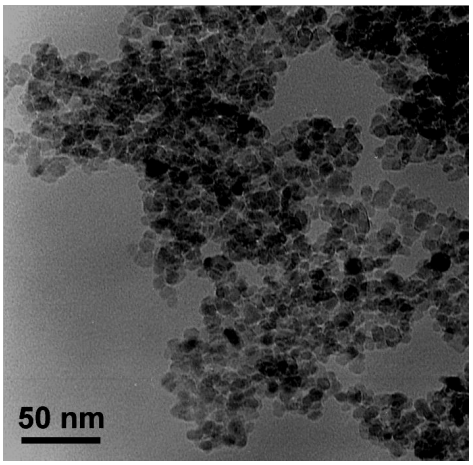

Fig. 9. TEM image of the doped TiO_2:Ni aerogel. The mesospheres dimension is of about 11 nm.

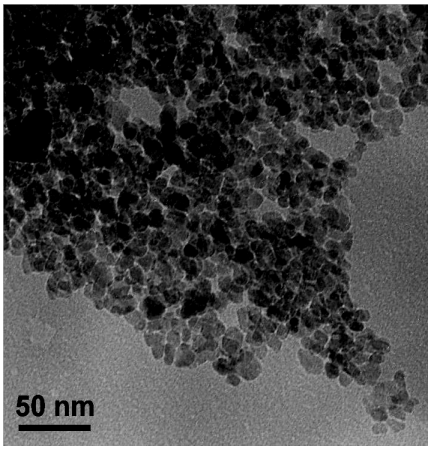

Fig. 10. TEM image of the doped TiO_2:Ag aerogel . The mesosphere size is of about 12 nm.

4. Conclusions

Different types of TiO_2 aerogels have been successfully synthesized and the sample with the highest BET surface area was morphologically characterized with the help of SEM measurements. Because of their ultra low density, high homogeneity and high surface area, TiO_2 aerogels are attractive for their applications in solar energy conversion, photocatalysis. Structural and dimensional investigations of this aerogel sample heat-treated for two hours at temperatures between 300 and 600 ^{0}C have been performed by means of SAXS, Raman and XRD techniques.

The photoelectrochemical percolation efficiency in DSSC electrodes is increased by ruthenium-bipyridil complexes and by their supramolecular assemblies with porphyrins prepared.

A serie of ZnO-TiO_2 aerogels were prepared by the sol-gel method followed by supercritical drying. By varying the ZnO quantity (1-10 %) and the nature of Zn precursors - zinc (II) nitrate hexahydrate and zinc (II) acetylacetonate see Table 2), an extensive study has been performed.

Mesoporous metal doped titania thin films, made by a sol-gel method are structured in nanoparticles of controlled and uniform size, both in pure form or doped with silver, nickel and iron. In the TiO_2:Fe doped films it can be presumed that Fe^{3+} substitutes Ti^{4+} preferentially on the body centered and face centered lattice sites in the anatase structure.

Acknowledgements

This work was supported by the Ministry of Education and Research through MENER program, HYDROSOL project No. 710/24.072006. We thank to DEGUSSA A.G.- GERMANY for sponsoring the research team with Degussa P25 titania.

References

[1] A. Fujishima, K. Honda, Nature **238**, 37 (1972).
[2] J. Nowotny, C.C. Sorrell, L.R. Sheppard, T. Bak, Int. J. Hydrogen Energy **30**, 521–544 (2005).
[3] M. Ciszkowska, M. Tomkiewicz, Curr. Topics Electrochem. **8**, 1-5 (2001).
[4] M.R. Wasiliewski, Chem. Rev. **92**, 435-461(1992).
[5] D. Gust, T. A. Moore, A. L. Moore, Acc. Chem. Res. **34**, 40-48 (2001).
[6] C.-Y. Wang, C.-Y. Liu, in: A. Hubbard, S. Barbara (Eds.), Encyclopedia of Surface and Colloid Science, Marcel Dekker, NY, pp. 4926 (2002).
[7] C.-Y. Wang, C.-Y. Liu, X. Zheng, J. Chen, T. Shen, Colloids Surf. A, **131**(1–3), 271 (1998).
[8] C.-Y. Wang, C.-Y. Liu, J. Chen, T. Shen, J. Colloid Interface Sci. **191**, 464 (1997).
[9] Y. Cao, X. Zhang, W. Yang, H. Du, Y. Bai, T. Li, J. Yao, Chem. Mater. **12**, 3445 (2000)
[10] H. Tada, A. Hattori, Y. Tokihisa, K. Imai, N. Tohge, S. Ito, J. Phys. Chem. B, **104**, 4585 (2000).
[11] J. A. Wang, R. Limas-Ballesteros, T. Lopez, A. Moreno, R. Gomez, O. Novaro X. Bokhimi, J. Phys. Chem. B, **105**, 9692 (2001).
[12] A. Barau , M. Crisan, M.Gartner, V.Danciu, V. Cosoveanu, I.Marian, M. Anastasescu, M.Zaharescu, Mat. Sci. Forum **492-493**, 311 (2005).
[13] A. Barau , M. Crisan, M. Gartner, A. Jitianu, M. Zaharescu, A. Ghita, V. Danciu, V. Cosoveanu, I. Marian, J. Sol-Gel Sci. Techn. **37**, 175 (2006).
[14] R. Pirard, B. Heinrichs, J-P. Pirard, USA Patent **6**,307,116 /Oct. 10 (2001).
[15] X. Hu, S. Ji, R. Zhang, W.M. Risen, USA Patent **6**, 303, 046 /Oct. 16 (2001).
[16] V. Danciu, V. Coşoveanu, A. Peter, I. Marian, P.Marginean, E. Indrea, Annals of West University of Timisoara, Series Chemistry **12**,1029 (2003).
[17] G. Kodis, P. A. Liddell, L. de la Garza, P. C. Clausen, J. S. Lindsey, J. Phys. Chem. A **106**, 2036 (2002).
[18] A. F. Nogueira, A.L.B. Formiga, H.Winnischofer, M. Nakamura, F. Engelmann, K. Araki; H.E. Toma, Photochem. & Photobiolog. Sci. **3**(1), 56 (2004).
[19] I. C. Ladiu, V. Danciu, V. Cosoveanu, A. Rustoiu-Csavdari, P. Lianos, Rev. Roum. Chem. **47**(12), 1247 (2002).
[20] Ph. Dieudonné, P. Delord, J. Phalippou, J.Non-Cryst. Solids **225**, 220 (1998).
[21] J.A.Lake, Acta Crystallogr. **23**, 191 (1967).
[22] L. Baia, A. Peter, V. Cosoveanu, E. Indrea, M. Baia, J. Popp, V. Danciu, Thin Solid Films **511-512**, 512 (2006).
[23] A. Hagerfeldt, M. Grätzel, Chem Rev. **95**, 49-55 (1995).
[24] A. Emmerling, J.Frike, J.Non-Cryst. Solids **145**, 113 (1992).
[25] L.A.Chiavacci,K.Dahmouche,V.Boris,C.V.Santilli, V. de Zea Bermudez, L.D.Carlos, J.Appl.Cryst. **36**, 405 (2003).

[26] P. V. Konarev, V. V. Volkov, A. V. Sokolova, M. H. J. Koch, D. I. Svergun, J. Appl. Cryst. **36**, 1277 (2003).
[27] E. Indrea, S. Dreve, T.D. Silipas, MATNANTECH Workshop, Jupiter, Romania, June (2005).
[28] E. Fagadar-Cosma, C. Enache, Gh. Fagadar-Cosma, C. Savii, J. Optoelectron. Adv. Mater. **9**(6), 1878 (2007).
[29] K. Pasquier, J. Phys. Chem. B **107**, 597 (2003).
[30] W. Kraus, G. Nolze, J. Appl. Crystallogr. **29**, 301 (1996).
[31] E. Indrea, Adriana Barbu, Appl. Surf. Sci. **106**, 498 (1996).
[32] N. Aldea, E. Indrea, Comput. Phys. Commun. **60**, 155-159 (1990).

*Corresponding author: eindrea@s3.itim-cj.ro